Journal of Neuroscience Methods 422 (2025) 110514

Contents lists available at ScienceDirect

Journal of Neuroscience Methods

journal homepage: www.elsevier.com/locate/jneumeth

Flexible modeling of large-scale neural network stimulation: Electrical and optical extensions to The Virtual Electrode Recording Tool for EXtracellular Potentials (VERTEX)

Anne F. Pierce [a,b], Larry Shupe [c], Julien Bloch [a,b], Eberhard Fetz [b,c], Azadeh Yazdan-Shahmorad [a,b,d,*]

[a] Department of Bioengineering, University of Washington, Seattle, WA 98195, USA
[b] Washington National Primate Research Center, Seattle, WA 98195, USA
[c] Department of Physiology and Biophysics, University of Washington, Seattle, WA 98195, USA
[d] Department of Electrical and Computer Engineering, University of Washington, Seattle, WA 98195, USA

ARTICLE INFO

Keywords:
Neural Modeling
Electrical stimulation
Optogenetic stimulation
Paired Pulse stimulation
Patterned stimulation
Closed-loop stimulation
Neural simulation

ABSTRACT

Background: Computational models that predict effects of neural stimulation can serve as a preliminary tool to inform *in-vivo* research, reducing costs, time, and ethical considerations. However, current models do not support the diverse neural stimulation techniques used *in-vivo*, including the expanding selection of electrodes, stimulation modalities, and stimulation protocols.

New method: We developed several extensions to The Virtual Electrode Recording Tool for EXtracellular Potentials (VERTEX), the MATLAB-based neural stimulation tool. VERTEX simulates input currents in a large population of multi-compartment neurons within a small cortical slice to model electric field stimulation, while recording local field potentials (LFPs) and spiking activity. Our extensions enhance this framework with support for multiple pairs of parametrically defined electrodes and biphasic, bipolar stimulation delivered at programmable delays. To support the growing use of optogenetic approaches for targeted neural stimulation, we introduced a feature that models optogenetic stimulation through an additional VERTEX input function that converts irradiance to currents at optogenetically responsive neurons. Finally, we added extensions to allow complex stimulation protocols including paired-pulse, spatiotemporal patterned, and closed-loop stimulation.

Results: We demonstrated these novel features using VERTEX's built-in functionalities, with results consistent with other models and experimental work.

Comparison with existing methods: Unlike other tools, our extensions enable both electric field and optogenetic stimulation, provide a range of open- and closed-loop protocols, and offer flexible settings within a large-scale cortical network of neurons with realistic biophysical properties.

Conclusions: Our extensions provide an all-in-one platform to efficiently and systematically test diverse, targeted, and individualized stimulation patterns.

1. Introduction

Neural stimulation has significant history and promise for treating neurological disorders characterized by damaged or aberrant neural activity, such as movement disorders, epilepsy, and stroke. However, the effectiveness of stimulation-based treatments has variable outcomes across clinical and preclinical trials. This inconsistency is attributed to the use of non-individualized stimulation and diverse methods employed across experiments, including variations in electrode types, spatial and temporal stimulation dynamics, and open versus closed-loop approaches. While it is critical to investigate methods that consistently yield optimal outcomes, *in-vivo* experiments are time-intensive, expensive, and raise ethical considerations regarding the use of humans and animals. Consequently, before conducting *in-vivo* experiments, computational modeling can be used as a fast and cost-effective method to predict effects of stimulation under various conditions. The results could inform and reduce the number of subsequent *in-vivo* experiments, and aid in the development of reliable, individualized, and targeted

* Corresponding author at: Department of Bioengineering, University of Washington, Seattle, WA 98195, USA.
E-mail address: azadehy@uw.edu (A. Yazdan-Shahmorad).

https://doi.org/10.1016/j.jneumeth.2025.110514
Received 15 January 2025; Received in revised form 27 May 2025; Accepted 12 June 2025
Available online 13 June 2025

therapeutic treatments.

While existing software can predict effects of neural stimulation, most models simulate neural activity in large populations of neurons lacking realistic biophysical properties or simulate activity in only a few neurons that possess complex, neurophysiological characteristics. Since *in-vivo* neural stimulation induces both local and network-wide effects that contribute to its therapeutic outcomes, it is crucial to have a model suited for an extensive network of neurons while maintaining realistic properties. The Virtual Electrode Recording Tool for EXtracellular Potentials (VERTEX) is a MATLAB-based software designed to simulate local field potentials (LFPs) and spike timing in response to electrical stimulation in a large population of neurons within a multi-layer slice of cortex (Tomsett et al., 2015; Thornton et al., 2019). VERTEX simulates neuron types, compartments, densities, and connectivity properties based on empirical research, which lends to realistic neuron characteristics. Additionally, VERTEX generates neuron dynamics with the adaptive exponential integrate and fire (AdEx) model (Brette and Gerstner, 2005), which can mimic the firing patterns of many different neuronal cell types. Together these features achieve a balance between complexity and practicality to give rise to realistic spiking patterns and LFP calculations, making VERTEX uniquely suited to efficiently test the effects of electrical stimulation-based approaches in a slice of cortex prior to *in-vivo* experiments.

However, VERTEX has constraints that hinder its ability to model the wide range of approaches used *in-vivo*. These include a restrictive and cumbersome electrode design process, a suboptimal electrical stimulation waveform, a single stimulation modality, and few stimulation protocols. To overcome these limitations, we developed several extensions to VERTEX to broaden its capabilities. We first developed a new script that enables electrical stimulation with biphasic waveforms and facilitates rapid creation and modification of electrode shape, number, and positioning. Next, we created a model to simulate optogenetic stimulation by converting irradiance to input current. This represents a significant advancement since optogenetics has become a highly prevalent method to deliver targeted stimulation. Finally, we added the capability to deliver three stimulation protocols including paired-pulse stimulation, spatiotemporal patterned stimulation, and closed-loop stimulation. We demonstrate our novel extensions using VERTEX's built-in spiking and LFP recordings. These novel features allow users to test a vast array of stimulation approaches, providing a highly adaptable LFP simulation tool.

2. Materials and methods

All simulations used the following settings unless otherwise noted. The size of the simulated tissue block was 1.5 × 1.5 × 2.6 mm deep with virtual electrodes for LFP recording sites spaced in a 3 × 3×6 grid to capture activity in each cortical layer. We used the 15 neuron-group VERTEX model developed by Tomsett et al. (2015), which incorporates the biophysical and connectivity patterns of 15 distinct types of cortical neurons, each characterized by unique features such as compartmental structure, soma location, projecting layer, firing rate, number of synapses and synapse dynamics. Our resulting networks contained approximately 224 thousand neuron units and 569 million connections. VERTEX calculates LFPs by summing the membrane potentials of each compartment, weighted by their distance from the virtual electrodes. Neuronal spiking is driven by synaptic and stochastic input currents to the AdEx integrate and fire model (Brette and Gerstner, 2005) that VERTEX employs for each neuron unit. The means and standard deviations of the stochastic currents used in Tomsett et al. (2015) result in large gamma oscillations that can mask other evoked potentials. To reduce the model's inherent gamma oscillations to levels low enough to not obscure stimulus-evoked LFPs, we chose to scale the means and standard deviations of the stochastic currents by 1.125x and 1.75x respectively. These values were found by evaluating simulations employing different values and comparing the resultant LFP power spectrums and neuronal spiking distributions to empirical data (Bloch et al., 2023). Simulations were run remotely on the Neuroscience Gateway (Sivagnanam et al., 2013) computer cluster or on a local PC (AMD 7800X3D CPU with 128 GB memory) and generally required about 1 h run time per 1 s of simulated time to complete. A list of added or modified code modules are reported in Supplementary Table 1.

2.1. Electric field stimulation: parametric electrodes and biphasic stimulation

VERTEX has built in support for electric field stimulation with demonstration code for monophasic stimulation through a single pair of differential electrodes positioned horizontally through the model tissue slice. The 3D electrode topology is created in an external 3D modeling application and imported into MATLAB (Mathworks Inc., Natick, MA, USA). The reliance on separate software requiring multiple cumbersome steps limits rapid modification and parameterization of electrodes. To overcome this limitation, we implemented a new script for electric field stimulation that removes the dependence on an external 3D application. A function called within this script parametrically creates electrode topologies directly in MATLAB, allowing easy modification of the electrode shape, the number of electrode pairs, and the positioning of the electrodes within the tissue volume. This function generates the same format of tessellated 3D geometry that VERTEX would otherwise import from an external application and that is used by MATLAB's Partial Differential Equation (PDE) Toolbox to build a finite element model of the electric potential in the tissue volume resulting from a potential difference between the electrodes (Thornton et al., 2019). We demonstrate the benefit and versatility of this user-friendly feature with single and multiple pairs of tapered tip and surface patch electrodes oriented perpendicular to the ventral surface of the modeled tissue, resembling electrodes in the Utah Array or an Electrocorticography (ECoG) array (Fig. 1).

Additionally, in this script we introduce features that significantly expand the range of stimulation options. For example, we add the ability to modify stimulation timing and pulse parameters during an ongoing simulation, a feature particularly beneficial for closed-loop stimulation. Lastly, rather than restricting stimulation to a single pair of differential electrodes with monophasic waveforms, our code accommodates multiple pairs of stimulating electrodes that allow biphasic, bipolar stimulation. This stimulation waveform is more commonly used in clinical settings, as it is less likely to cause abnormal neuronal activity, tissue damage, and electrode degradation compared to monophasic stimulation (Yuan et al., 2021). We perform biphasic stimulation by inverting the electric field halfway through the stimulus duration. While this is constant voltage stimulation, the VERTEX tissue model is purely resistive and the current applied can be estimated from the tissue conductivity, electrode surface area, and the electric field calculated by MATLAB's PDE Toolbox. These novel features broaden the range of electrode and stimulation settings available, facilitating comprehensive investigations into effective parameters for modulating neural activity.

2.2. Modeling optogenetic stimulation

Optogenetics has become a commonly used technique to rapidly modulate neural activity in neurons expressing exogenous light-sensitive ion channels. By applying light to the targeted region, the light-sensitive ion-channels open and induce a photocurrent in the affected cells. We created a novel script to model optogenetic stimulation using VERTEX's built-in functionality for adding input currents to neuron units. These currents can vary with time and may be turned on and off to model photocurrents. Light-sensitive units are defined in the script, allowing users to specify which cell types or layers to set as light-responsive. The light source for optogenetic stimulation is typically a laser which projects light of a specific wavelength through an optical fiber. The laser's radiant power (P in mW) and the fiber's radius (r in

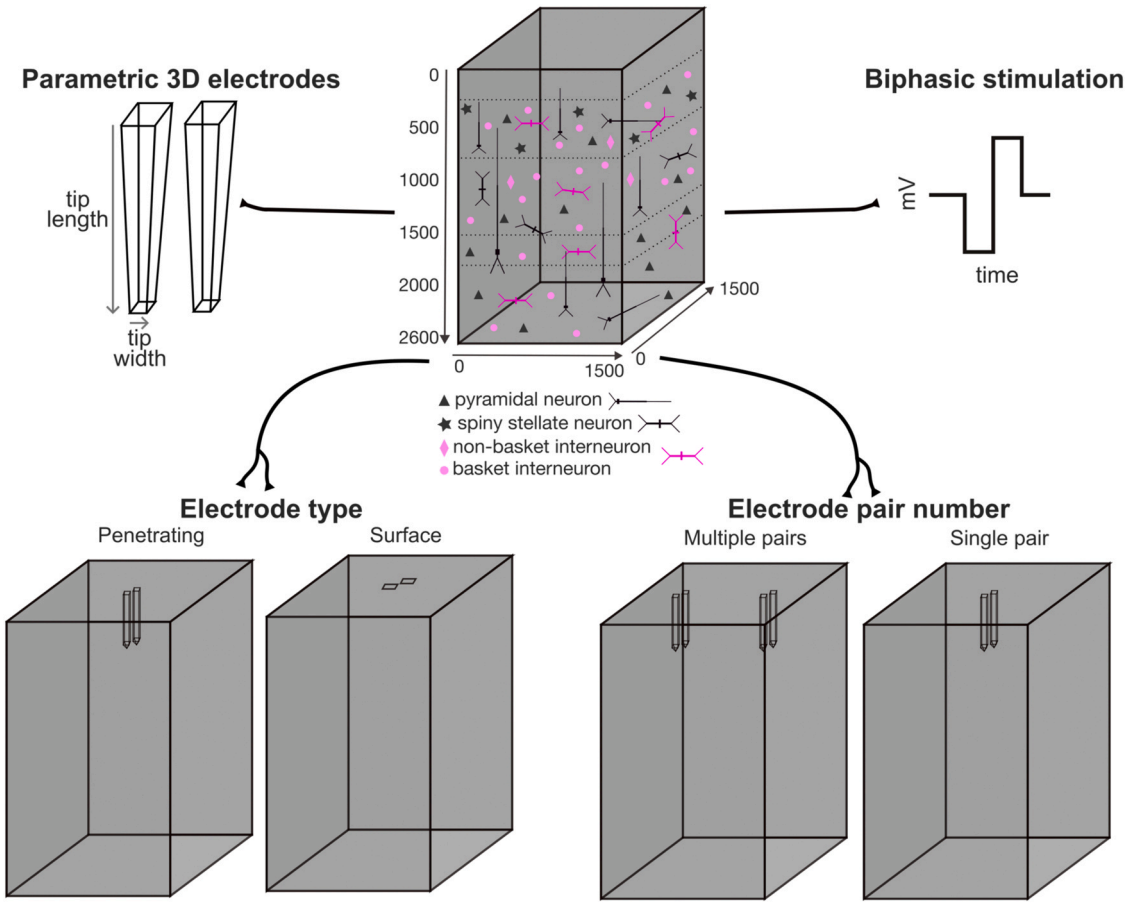

Fig. 1. Added features for electric field stimulation. VERTEX defines a tissue volume where a variety of modeled neuron types are placed. We introduce several features to increase flexibility and versatility when defining electrode and stimulation parameters in the tissue volume. Electrode positions, lengths, and widths are parametrically defined. The electrode geometry can represent penetrating or surface electrodes in a single pair or multiple pair configuration. Biphasic stimulation is modeled by inverting the electric field halfway through the pulse duration.

mm) are additional user-defined parameters in the script and control the intensity of the stimulation with the initial irradiance (E_0) at the tissue surface beneath the optic fiber defined by Eq. 1.

$$E_0 = \frac{P}{\pi r^2} \tag{1}$$

$$f(z) = \frac{e^{\left(\frac{-z}{\tau}\right)}}{1 + a z^2} \tag{2}$$

$$E(x,y,z) = E_0 \quad f\left(\sqrt{l^2 + z^2}\right), \quad l = h \quad \sqrt{x^2 + y^2} \tag{3}$$

Irradiance at depth (z) directly below the light source is modeled by fitting both an exponential and geometric decay to data from Yizhar et al. (2011), where an optical fiber was lowered through a tissue block to measure light transmission through unfixed brain tissue. The 10 % and 1 % light transmission contours provided the percentage of light remaining at depth and lateral distance from the optical fiber center point. The depth (z) of these contours is measured for both 473 nm and 594 nm light and fit to Eq. 2. The ratio (h) of depth to half-width (at half-depth) of the 1 % contours is used to calculate a scaled lateral distance (l) to create a 3-dimensional estimate of irradiance at any (x, y, z) coordinate offset from the center tip of the light source. Parameter fitting values are shown in Table 1 and the irradiance estimate (mW/mm^2) is shown in Eq. 3. When optical stimulation is initiated, irradiance values for each light source are calculated for each light-sensitive unit at its soma position.

There are several theoretical models for converting irradiance to photocurrents for various opsins. We chose Foutz et al. (2012) for modeling Channelrhodopsin-2 (ChR2) with 473 nm light because it demonstrated photocurrent responses across various neuronal compartments and irradiance levels. For Chronos and vfChrimson we selected models that offered a comprehensive investigation of photocurrent dynamics across several parameters - including pulse width and frequency, irradiance, and light wavelength - with results congruent with experimental work (Saran et al., 2018; Gupta et al., 2019). For Jaws, we relied on work from Chuong et al. (2014) as it provided experimental results for photocurrents elicited by various irradiance values. Peak photocurrent estimates (in picoamps) for irradiance levels E (in mW/mm^2) were fit with Eq. 4 for ChR2, Eq. 5 for Chronos, Eq. 6 for vfChrimson, and Eq. 7 for Jaws.

Table 1
Parameters for estimating irradiance at coordinate (x, y, z) in millimeters.

Parameter	Blue light (473 nm)	Amber light (594 nm)
τ	0.39 mm	0.38 mm
a	92	8.8
h	1.14	1.67

$$I_{chr2}(E) = 49.3 \quad E^{0.89} \tag{4}$$

$$I_{chronos}(E) = 2293 * \left(1 - \frac{1}{1 + 0.73E}\right) \tag{5}$$

$$I_{vfChrimson}(E) = 1279 * (1 - \frac{1}{1 + 1.7E}) \quad (6)$$

$$I_{jaws}(E) = \quad -1244 * (1 - \frac{1}{1 + 0.104E}) \quad (7)$$

Photocurrent dynamics are written into a VERTEX input model that handles optogenetic stimulation. This is a step function with exponential on and off dynamics to simulate the rise and fall of an input current to a precalculated value during the application of a light pulse. The time-constants used for the on and off mechanics for ChR2 are τ_{on} = 1.5 ms, τ_{off} = 11.6 ms (Mattis et al., 2012), for Chronos are τ_{on} = 0.65 ms, τ_{off} = 3.6 ms (Saran et al., 2018,) for vfChrimson are τ_{on} = 1.0 ms, τ_{off} = 2.7 ms (Gupta et al., 2019), and for Jaws are τ_{on} = 3.6 ms, τ_{off} = 4.2 ms (Chuong et al., 2014).

2.3. Stimulation paradigms

We created new scripts for three stimulation paradigms: paired-pulse, spatiotemporal patterned, and closed-loop stimulation. Each paradigm can use either electrical or optogenetic stimulation. Paired-pulse and spatiotemporal patterned stimulation both involve delivering stimulation at multiple sites with temporal delays between them. These spatial and temporal properties can induce spike-timing-dependent plasticity (STDP), a biological phenomenon based on spike timing differences between the postsynaptic unit (firing at time t2) and the presynaptic unit (firing at t1) with the spike-timing difference defined as $\Delta t = t2 - t1$. Positive differences strengthen while negative differences weaken connectivity between the pre- and postsynaptic unit. STDP is built into VERTEX synapse models to allow changes in connection strengths between units. In this STDP implementation, each time the pre- or postsynaptic neuron fires, there is an update to synapse connectivity, where two exponential functions (per synapse), each with unique decay times for the pre- and postsynaptic neuron, dictate the degree of synaptic connectivity change.

Although VERTEX demonstrates a form of paired-pulse stimulation with STDP, it currently only supports paired-pulse stimulation using a single pair of electrodes at the same site, whereas paired-pulse stimulation is typically administered at separate sites. Since this paradigm does not represent the typical protocol used *in-vivo,* we created a novel script for paired-pulse stimulation where stimulation is applied at distinct sites. Additionally, we created a new script to deliver spatiotemporal patterned stimulation, where stimulation can be applied to a greater number of sites with varying amplitudes and pulse delays between sites.

The third paradigm we support is closed-loop stimulation, where stimulation is delivered in response to on-going activity. In biophysical experiments, stimulation can be administered in response to behaviors, neural activity such as LFPs or single unit activity, and peripheral activity including signals from electromyography. In VERTEX, closed-loop stimulation is largely limited to recorded LFPs and spike times. We have implemented two forms of closed-loop stimulation, both of which are dependent on LFP measurements. The first is cycle-triggered stimulation where a stimulus pulse is delivered based on the amplitude and phase of the filtered LFP recorded on a single recording electrode. The second closed-loop paradigm is amplitude-adjusted stimulation where the amplitude of stimulation is adjusted to keep the magnitude of an LFP channel within a certain range. Both methods require transferring partial LFP values between the parallel MATLAB processes used to accelerate VERTEX so that each process has a complete copy of the LFP at each recording site.

3. Results

3.1. Optogenetic stimulation

To get an estimate of light penetration through the modeled tissue, we generated contour plots of irradiance at depth and lateral distance for 473 nm and 594 nm light using a single light source with a radius of 100 μm (Fig. 2A). Both contour plots have a dramatic drop-off in irradiance in the modeled tissue, though the fall-off of 594 nm irradiance is more gradual compared to 473 nm. The depth of light penetration shown here for 473 nm and 594 nm light is consistent with previous *in-vivo* work, reflecting greater tissue penetration with longer wavelengths due to reduced light absorption and scattering (Senova et al., 2017). Our models for converting irradiance to current are demonstrated in Fig. 2B. For each of the four modeled opsins - ChR2, Chronos, vfChrimson, and Jaws - we show current induced by a 5 ms light pulse across several irradiance values. In accordance with biophysical experiments, we found Chronos to have high sensitivity at low irradiance values (Klapoetke et al., 2014). To highlight the diverse effects of optogenetic stimulation on spiking activity and LFP generation across the different opsins, we show simulations for each opsin under identical stimulation parameters (Fig. 2C). Each simulation displays the spiking and LFP response following a 5 ms light pulse, where all units were set as light-responsive, averaged across 100 pulses. Each simulation used a light power of 7.2 mW and radius of 100 μm. To calculate tissue maps of spike-rate changes evoked by stimulation, unit spike times were divided spatially into 25 μm bins based on soma positions within the tissue volume. Baseline spiking rates were calculated for each bin by summing spike counts along either the Z axis (top-down view) or Y axis (side--view) for the 50 ms time-window preceding stimulus onset times. Spike-rate responses were similarly calculated for the 5 ms stimulus duration. Percent increases in spiking were plotted on log scales to highlight smaller changes and averaged across the 100 pulses delivered. These maps are shown from top-down (top row) and side-view perspectives (middle row). Differences in firing rates between layer boundaries, which are apparent in the side-view perspectives, result from each neuron group's somas lying entirely within their respective layers and having unique firing characteristics and connectivity.

Additionally, we show the stimulus-aligned LFP from the electrode located at the surface-center of the tissue model, directly under the light source, averaged across 100 pulses (bottom row). We quantified the stimulus response strength using 3 measures - percent spiking increase, LFP peak to peak, and the LFP root mean square (Fig. 2D). Percent spiking increase was calculated by counting all spikes in the tissue model within a 5 ms window before and after stimulation. For each stimulation, we computed the following: ((post-stimulation spike count – pre-stimulation spike count)/pre-stimulation spike count) X 100. The final value represents the average across all 100 stimulation pulses. For both the peak to peak and root mean square measures, we use the LFP from the center-surface electrode. We calculated the LFP peak to peak by subtracting the minimum LFP value from the maximum LFP value within 100 ms post-stimulation using LFP values averaged across all stimulations. We calculated the root mean square (RMS) of the LFP by first subtracting the mean of the LFP from the LFP values, squaring the result, and then summing those squared differences. The sum was then divided by the total number of values, and the square root of the result was taken. All three metrics showed significant differences between opsins (Kruskal-Wallis H test: % spiking increase $H(3) = 374.02$, $p = 9.38E\text{-}81$; LFP peak to peak $H(3) = 374.06$, $p = 9.38E\text{-}81$; LFP root mean square $H(3) = 374.06$, $p = 9.38E\text{-}8$. Post hoc Dunn's tests with Bonferroni correction revealed pairwise differences for all group comparisons (all groups $p < 5E\text{-}09$ for all metrics). Although ChR2 and Chronos simulations both used the blue-light model, Chronos stimulation evoked significantly greater spiking and LFP responses than ChR2 stimulation, which can be attributable to Chronos' increased light sensitivity and faster kinetics. While vfChrimson has lower light-

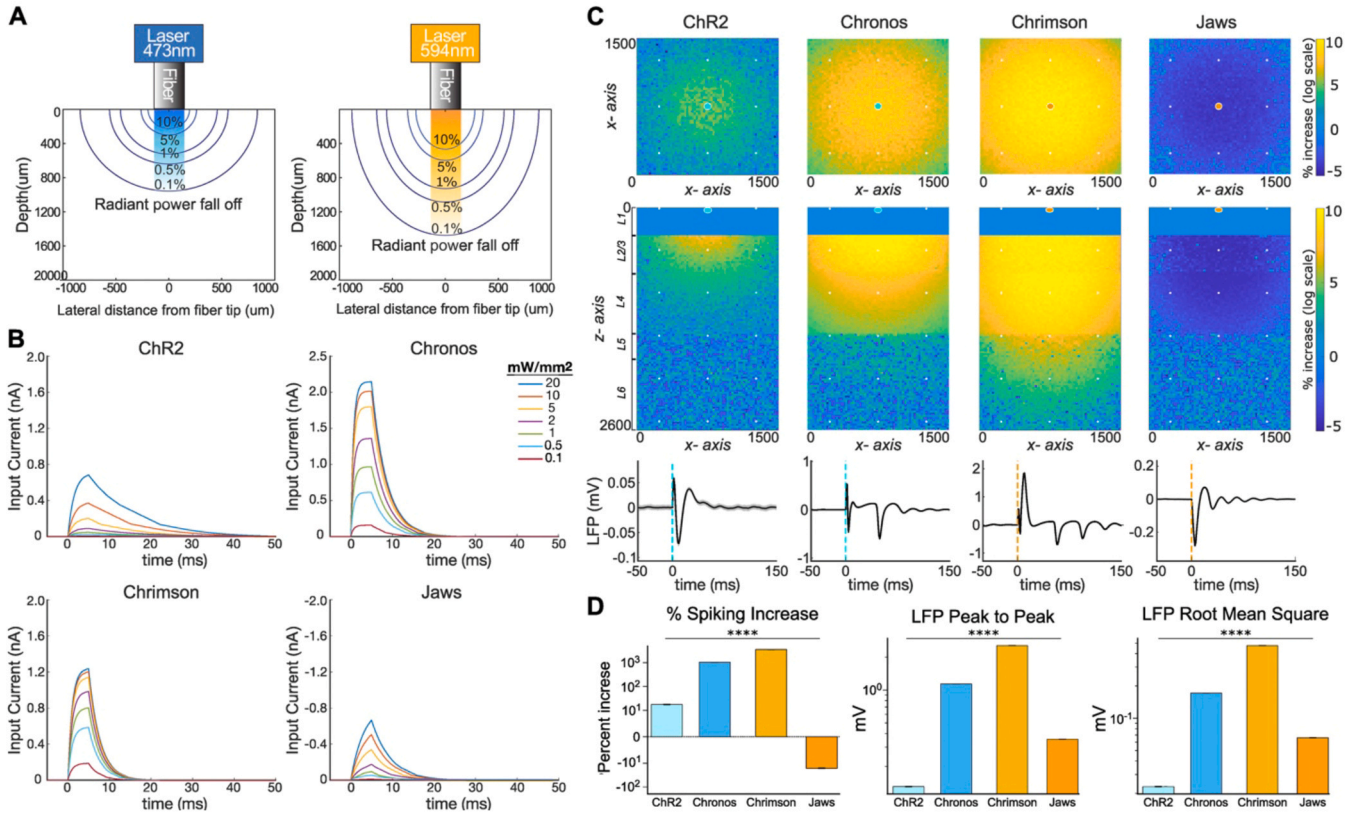

Fig. 2. Modeling optogenetic stimulation. A) light spread through tissue is modeled for blue light (473 nm) and amber light (594 nm) to determine photocurrent responses at different irradiance values. Radiant power fall-off is due to both light absorption and geometric fall-off with distance. B) photocurrent rise and decay are modeled for each of the four opsins using distinct exponential functions and are shown here in response to a 5 ms light pulse across several irradiance values. C-d) a simulation was run for each of the four opsins where 100 stimuli events were delivered. Each stimuli event consisted of a 5 ms pulse using the same optogenetic parameters (fiber radii = 100 μm; light power = 7.2 mW; all neuron unit groups set as light-responsive). the simulation modeling ChR2 and Chronos used the 473 nm/blue light model whereas the simulations modeling Chrimson and Jaws used the 594 nm/amber light model. C) the top-down (top row) and side-view (middle row) through the tissue show the percent change in spiking activity on log scales during the 5 ms of stimulation compared to a baseline period (50 ms prior to stimulation). White dots represent the location of the recording electrodes in the tissue slice. The bottom row shows the average LFP, with the standard deviation in gray shading, for the surface-center recording electrode with the baseline subtracted, averaged across 100 stimuli events. The vertical dotted lines represent the stimulation onset times. D) three measures of stimulus response strength with SEM error bars shown in 2D: percent increase in spiking during the stimulus (left), LFP peak to peak (middle), and root mean square (right) of the average surface LFP response during the 100 ms following the stimulus. All three metrics show significant differences between opsins (Kruskal-Wallis H test: % spiking increase $H(3) = 374.02$, $p = 9.38E\text{-}81$; LFP peak to peak $H(3) = 374.06$, $p = 9.17E\text{-}81$; % spiking increase $H(3) = 374.06$, $p = 9.17E\text{-}81$. ****$p < 0.0001$.

sensitivity than Chronos, we found that vfChrimson activation led to increased spiking, spatial spread of spiking, and LFP responses. This enhanced response is likely due to the use of amber light for vfChrimson activation, which penetrates tissue more deeply compared to blue light activation used in the Chronos simulation. As expected for an inhibitory opsin, the Jaws stimulation resulted in decreased spiking activity and a negative change in LFP responses.

In addition to selecting which opsin to simulate, users can customize various stimulation parameters, including the light power, light radius, and which neuron unit groups to designate as light-responsive. Figure S1 demonstrates how modifying these parameters can influence spiking activity and LFP responses, with effects that range from subtle to pronounced. When examining light settings, we found that increasing the initial light power or decreasing the light radius, while maintaining the same light power, led to greater spiking activity, spatial spread of spiking, and LFP responses (Fig S1A-B). Additionally, in Figure S1D-E, we validated the ability of our model to allow cell type specific stimulation. When comparing vfChrimson activation in all units, excitatory units only, and inhibitory units only, we observed that excitatory units were primarily driving the maximum LFP response, whereas inhibitory units were regulating post-stimulation oscillations.

3.2. *Paired-pulse stimulation with spike-timing-dependent plasticity*

In Fig. 3, we demonstrate our paired-pulse stimulation paradigm, combined with several of our extensions to electric field stimulation, including biphasic stimulation at multiple electrode pairs with a programmed delay. In this simulation we enabled VERTEX's built in STDP feature that requires using a script where defined STDP parameters govern the temporal dynamics and degree of connectivity change. Based on work shown in Bi and Poo (2001), we set the decay time constants for the exponential curves to 17 ms and 34 ms for positive and negative Δt respectively such that small values of Δt give the largest changes and large values of Δt give exponentially smaller changes (Fig. 3A). To provide slightly more area under the weakening curve, we set the amplitude for the weakening function to 0.53 times that of the curve for the strengthening function. This value was selected after testing various amplitudes and observing their effects on connectivity changes (Fig S2). We found that a value of 0.53 prevented runaway increases in connectivity strengths due to random activity since there is no homeostasis function, while also limiting unintended changes in connectivity outside the stimulation sites. This parameter is user-adjustable, as the optimal value may vary depending on the type of stimulation. The maximum change can be modified but is normally set between 0.001 and 0.005

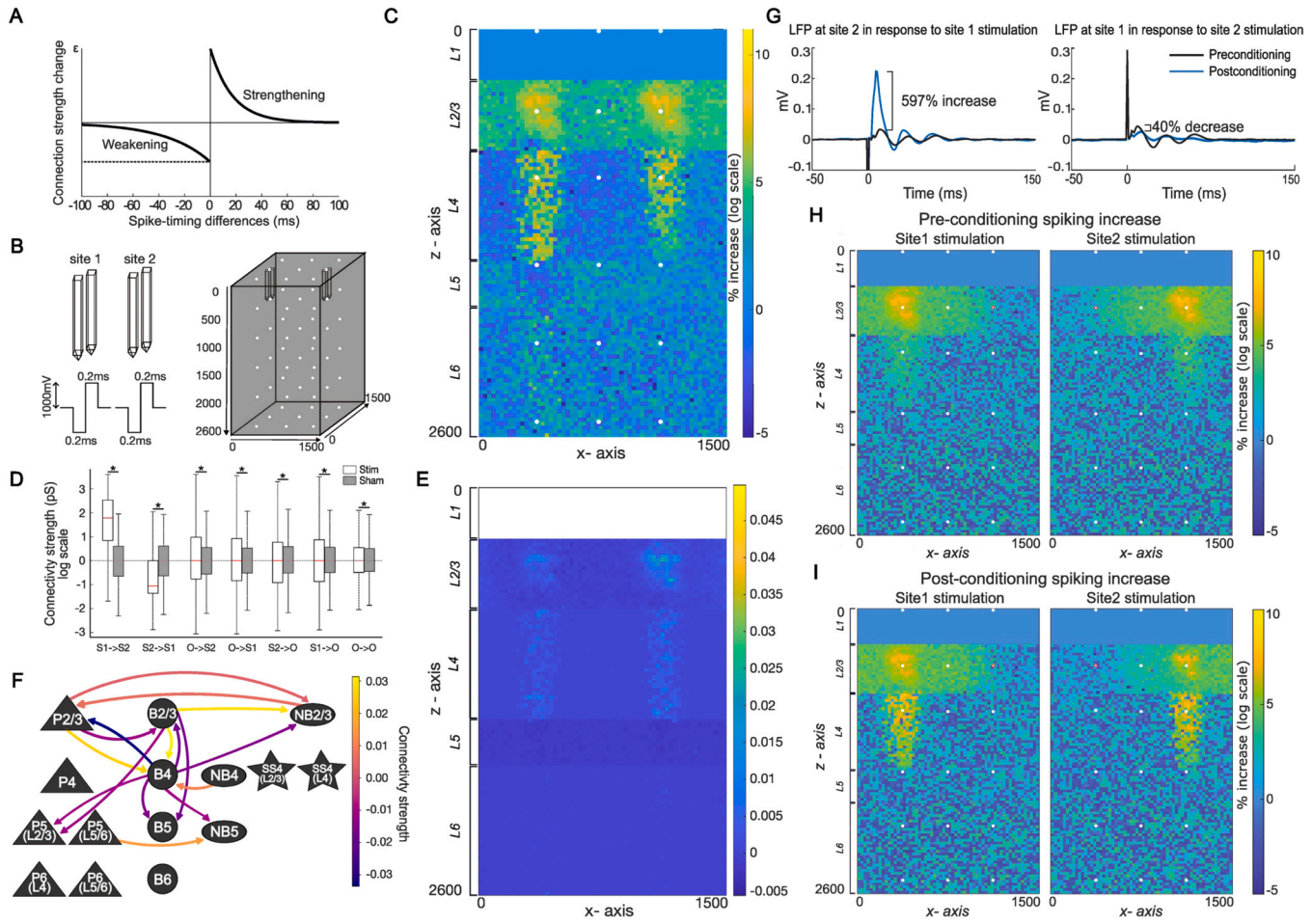

Fig. 3. Paired-pulse conditioning. A) schematic of STDP principle. ε Represents the largest possible weight change for any pair of spikes. We use 0.005 nanosiemens. B) schematic of paired-pulse electric field stimulation and placement of stimulating (black outline) and recording electrodes (white dots) in the tissue slice. C) side-view of percent increase in spiking activity in log scale during the 10 ms window after the stimulus. D) mean connection strengths from Site1 (S1), Site2 (S2), or units outside (O) of S1 or S2, comparing a simulation with paired-pulse conditioning (Stim) to a simulation with plasticity enabled but no stimulation (Sham). All stim groups differed significantly from their corresponding sham control (Mann-Whitney *u* test with Bonferroni correction, all pairwise comparisons showed $p < 5.40E\text{-}16$). Within the Stim condition, compared to connections between outside units (O -> O), connections from S1 to S2 significantly increased, while those from S2 to S1 significantly decreased, (Kruskal-Wallis H test: $H(6) = 87299.20$, $p < 0.0001$. Post hoc Dunn's tests with Bonferroni correction revealed $p < 0.0001$ for all pairwise comparisons). Dotted, horizontal line at zero. *$P < 0.0001$. E) side-view of connection strength changes showing the largest changes occur to units within 100 μm radius of the site's (x,y) locations in both layer 2/3 and layer 4. F) neuron groups (arranged vertically by cortical layer), showing only the top 5 % largest increases or 5 % largest decreases in mean connection-strength. "P" = pyramidal neuron, "B" = basket interneuron, "NB" = non-basket interneuron, "SS" = spiny stellate neuron. Layer abbreviations within parentheses represent the projection layer. G) stimulus evoked LFP responses for electrodes in layer 2/3 (outlined in red in 3H-I) for both the preconditioned and post-conditioned network. H) increased spiking activity in the 5 ms window after test stimulation for each site in the pre-conditioned and I) post-conditioned networks.

nanosiemens (nS). For the simulation in Fig. 3, we use 0.005 nS. Connection magnitudes can be limited and are normally restricted to the range between 0.001 and 4.0 nS.

In Fig. 3 we used VERTEX's original parameters for the stochastic input-current to the AdEx integrate-and-fire model since plasticity reduces the network's inherent oscillations to levels low enough to not obscure the stimulus-evoked responses. This also allowed for larger stimulus responses in deeper layers which resulted in brief oscillatory activity that dampened out within 100 ms. Network connection strengths were initialized from the results of running a non-stimulating network for 30 s with STDP turned on, allowing the paired-pulse conditioning to begin with a more stable distribution of connection strengths and very low LFP oscillations.

Paired-pulse conditioning was simulated using electric field stimulation at two sites separated by 750 μm in the middle of layer 2/3 (Fig. 3B). The electrode tips were modeled after a commonly used microelectrode array and used 50 μm tip lengths and 35 μm base diameters. The bipolar tips were placed 100 microns apart. 100 paired stimulation events were delivered where stimulation at the second site was delayed 5 ms from the first. 1000 mV biphasic-bipolar stimulation was delivered to each site in brief 0.4 ms pulses (0.2 ms each phase). This produced an estimated constant current stimulation of 65 μA at each site since the VERTEX tissue model is purely resistive.

Stimulus times were used to calculate post-stimulus changes in spiking activity (Fig. 3C), similar to graphs for optogenetic stimulation in Fig. 2 and S1. To capture effects at both sites in Fig. 3C, spike-rate responses were calculated for 0–10 ms after stimulation at the first site. Network connection strengths were saved before and after paired-pulse conditioning. Fig. 3D shows changes in connection strength after conditioning (post – pre) across different sites within the tissue model for two simulations, paired-pulse conditioning (Stim) and a separate control simulation that had plasticity enabled but without stimulation (Sham). Somas in layer 2/3 located within a 100 μm radius of the centerline of the first stimulating electrode were classified as "Site1" units, and the same criterion was used to classify somas near the second stimulating electrode as "Site2" units. All other somas were designated

as "Outside" either site. All Stim groups are significantly different from their corresponding Sham group (Mann-Whitney *U* test with Bonferroni correction, all pairwise conditions show $p < 5.4E-16$). These results are consistent with prior work demonstrating that paired-pulse stimulation can induce plasticity across large-scale cortical networks (Bloch et al., 2022; Yazdan-Shahmorad et al., 2018). Within the Stim condition, compared to outside units (O → O), there is a significant increase in connection strength from Site1 to Site2, and a significant decrease from Site2 to Site1(Kruskal-Wallis H test: $H(6) = 87299.20$, $p < 0.0001$. Post hoc Dunn's tests with Bonferroni correction revealing $p < 0.0001$ for all pairwise comparisons). Fig. 3E provides a layer-by-layer view of connection strength changes, revealing the largest increases concentrated near the stimulating electrodes and extending downward through layer 4 in a column beneath the stimulation sites. Additionally, there is a small, but uniform decrease in connection strength in layer 5. We then examined changes across specific neuron groups following paired-pulse conditioning, shown in Fig. 3F. This figure displays only the connections between neuron groups exhibiting the top 5 % greatest increases or bottom 5 % greatest decreases in connection strength. This figure highlights VERTEX's utility in providing simulation insights by soma location and neuron group.

After examining changes induced by paired-pulled conditioning, we then assessed responses to a single pulse stimulation at Site 1 or Site 2 (Fig. 3G-I) using the pre- and post-conditioning network connection strengths. Specifically, we examined the average LFP response recorded from the electrode in layer 2/3 nearest Site2 or Site1, respectively, after 100 single pulse stimulation trials at Site1 or Site2. After conditioning there was a 597 % increase in the LFP peak value at Site2 in response to Site1 stimulation (Fig. 3G, left column), and a 40 % decrease in LFP peak value at Site1 in response to Site2 stimulation (Fig. 3G, right column). These changes in LFP amplitude are reflected in the spiking activity observed in layer 2/3 (Fig. 3H-I). Notably, while post-conditioning stimulation at Site1 and Site2 produced opposite effects in layer 2/3, stimulation at both sites led to increased spiking activity in layer 4 (Fig. 3I).

3.3. Spatiotemporal patterned stimulation

In Fig. 4 we illustrate a simulation using our extensions for spatiotemporal patterned and optogenetic stimulation. Four optogenetic stimulation sites are placed in each of the four surface quadrants of the tissue slice: lower-left, upper-right, lower-right, and upper-left (Fig. 4A). These sites were stimulated, in that order, by 5 ms light pulses, each separated by 15 ms between the start of each light pulse. We used the ChR2/473 nm light model with light sources of 100 μm radius. The initial light power was 7.2 mW for each light source and all neuron groups were set as optogenetically responsive (Fig. 4B). This train of pulses was repeated every 250 ms for 20 s, totaling 80 stimulation events. Fig. 4A shows the stimulus triggered spiking activity is centered at each site with small refractory responses visible at previous stimulation sites. Spiking activity after the fourth stimulation site is shown from the side-view (Fig. 4 C) and top-down view for individual layers (Fig. 4D). Graphs aggregating activity within individual layers show localized spiking activity during the stimulus to layer 2/3 and 4 with lingering refractory responses from the previous site on the right side of the tissue model within layers 4 and 5 in Fig. 4C-D. This aligns with experimental work showing that stimulation at the cortical surface reduced firing rates in deeper cortical layers (Yazdan-Shahmorad et al., 2011, 2013). Fig. 4E shows the stimulation-averaged LFP responses recorded from electrodes centered on the x-y plane in each cortical layer. The LFP response shows evoked potentials for each light pulse that do not completely decay before the next light pulse is delivered (Fig. 4E).

3.4. Cycle-triggered closed-loop stimulation

Fig. 5 shows a cycle-triggered closed-loop stimulation using our new features for electric field stimulation to deliver biphasic stimulation at a single pair of differential electrodes in layer 2/3 (Fig. 5A). To remove baseline signal-shift and reduce high-frequency noise, a 20–30 Hz band-pass filter was applied to the surface recording electrode used to trigger stimulation, outlined in red in Fig. 5A. Cycle-triggered stimulation can be delivered on a rising or falling LFP with two user-defined parameters, the refractory period and the magnitude threshold. The refractory period defines the minimum time interval between stimulation events, while the magnitude threshold specifies the value that the filtered LFP must cross to trigger stimulation. In Fig. 5 stimulation was triggered by a rising filtered LFP with a refractory period of 100 ms and a magnitude threshold of −5 μV (Fig. 5B). Similar to the paired-pulse conditioning in Fig. 3, 1000 mV biphasic-bipolar stimulation was delivered in brief 0.4 ms pulses. The simulation ran for 30 s, with stimulation applied only between 5 and 25 s of simulation time. Within these 20 s, the filtered LFP met criteria to trigger stimulation 47 times. Fig. 5C shows the stimulation-aligned LFP response from the electrode outlined in red in Fig. 5A. The LFP trace, averaged across stimulation events, illustrates both the pre-stimulus oscillation that triggered the stimulation and the stimulation evoked response that followed. The location of increased post-stimulus spiking-activity is centered on the stimulation site with activity spreading primarily through layer 2/3 (Fig. 5D).

4. Discussion

4.1. Novel extensions

We present novel extensions for VERTEX that enhance the software's ability to model a diverse range of *in-vivo* stimulation approaches. First, we introduce a script that adds several new features for electric field stimulation, including the ability to parametrically create 3D electrodes using built-in MATLAB functions. This eliminates the need for external 3D modeling software, allowing users to easily create and position different electrode shapes, such as patches on the cortical surface or tapered electrodes penetrating the tissue. Additionally, we implemented the ability to deliver biphasic instead of monophasic stimulation, a stimulation waveform commonly used clinically due to more precise spatial targeting, tissue safety, and electrode longevity. Finally, we enable stimulation with programmable delays, which can be used to deliver stimulation with complex temporal and spatial patterns that can induce synaptic plasticity. These added functionalities facilitate users to easily test various electrode types and stimulation settings to identify the approaches that produce results most similar to their targeted outcomes.

Another key feature we implemented is the ability to model optogenetic stimulation. Over the past twenty years, optogenetics has become a widely adopted neuroscience technique used to control neural activity with spatial and temporal precision (Deisseroth, 2015). While optogenetics is primarily used in preclinical research, experimentalists are beginning to adapt optogenetics for clinical trials (Gao et al., 2023). Our extension offers extensive parametrization, developed specifically to mimic the technical choices available to experimentalists. For example, we model optogenetic stimulation with four popular opsins - Channelrhodopsin2, Chronos, vfChrimson, and Jaws - each having their own biophysical advantages and limitations. For instance, longer wavelengths of light, such as 594 nm used for vfChrimson and Jaws for neuronal activation and inhibition, respectively, can penetrate the brain deeper than 473 nm used for ChR2 and Chronos activation. Equally important, a user may require tightly regulated temporal stimulation, making the fast on/off kinetics of the Chronos model desirable. Another method commonly employed *in-vivo* is to select an opsin with a promoter that targets specific cell types. We support this technical approach by allowing specification of which neuron groups are light-responsive, thereby enabling stimulation of specific cell types or layers. Thus, depending on the desired depth of stimulation, kinetics of each opsin, neuronal target, and available resources, users can modify variables that best meet their needs. To our knowledge, our extensions provide the

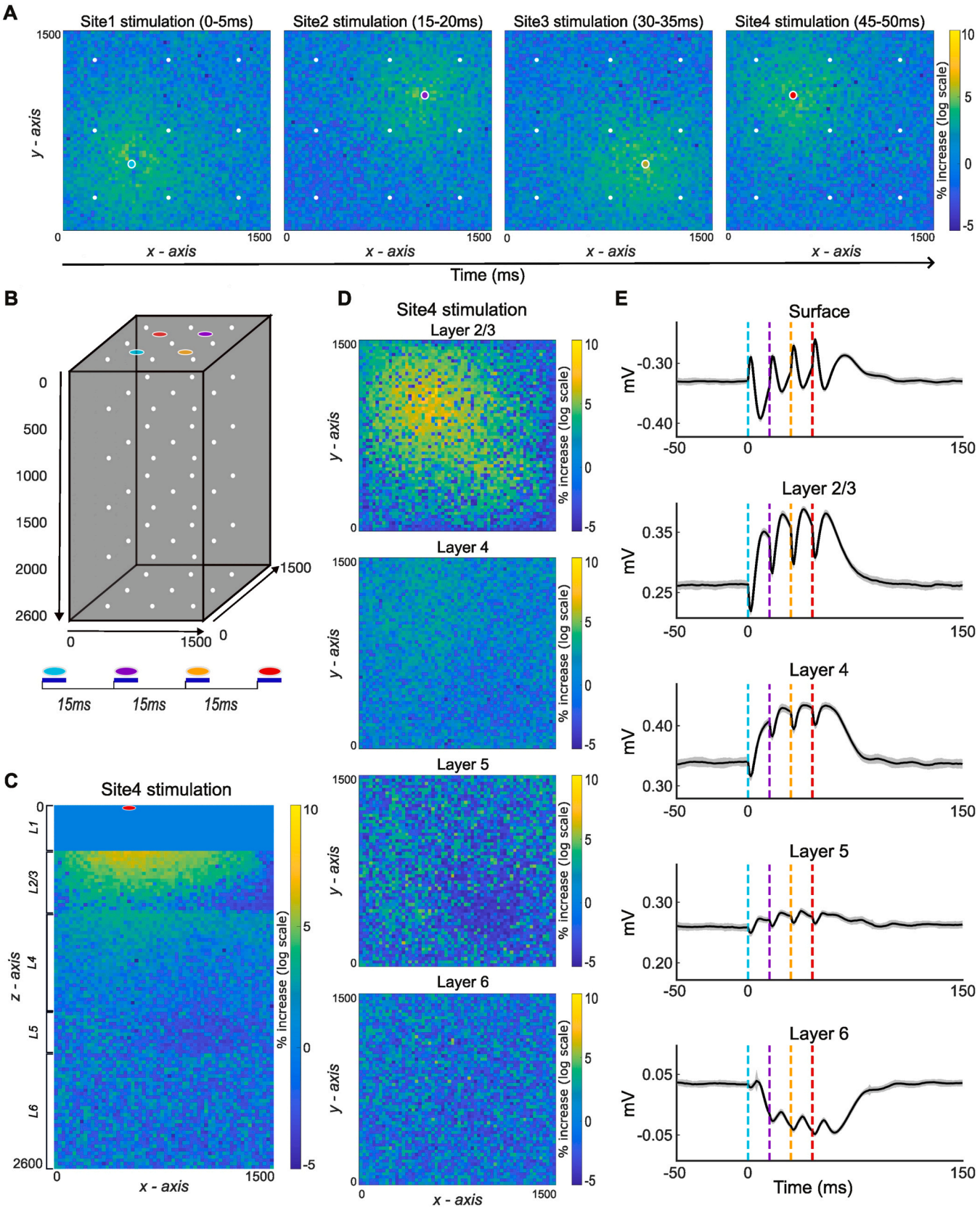

Fig. 4. Spatiotemporal patterned stimulation. A) top-down view of increased spiking activity on log scales in response to four consecutive optical pulses delivered at 15 ms intervals to different sites in the tissue slice. B) placement of each light source (colored dots) and recording electrodes (White dots) in the tissue slice. Timing of stimulation for each light pulse shown on bottom. Dark blue bars indicate 5 ms light pulse durations. C) side-view of increased spiking activity from the fourth stimulus site. D) top-down view of spiking activity aggregated by layer after stimulation at the fourth site. E) LFP averages aligned at the first pulse, with standard deviation in gray shading for the center column of recording electrodes. Dotted vertical lines represent stimulation onset times.

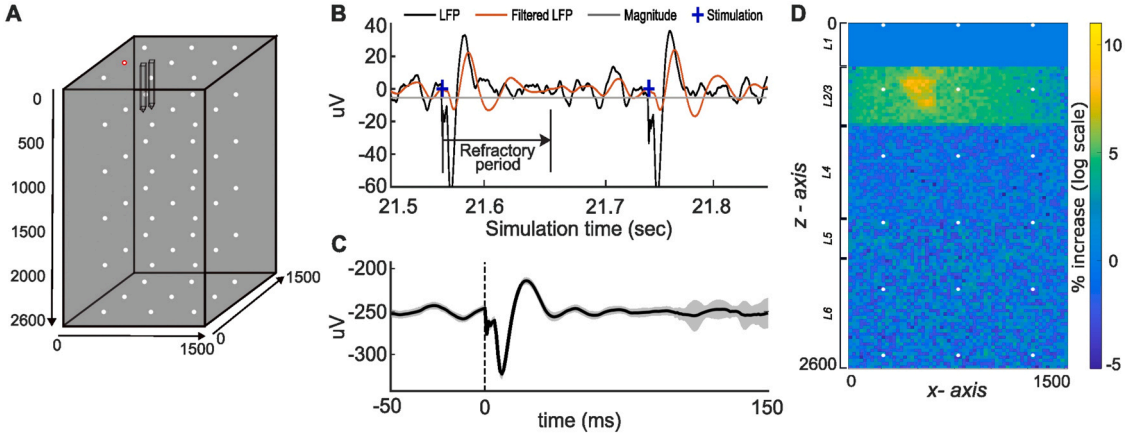

Fig. 5. Closed-loop stimulation. A) placement of stimulating (back outline) and recording electrodes (white dots) in the tissue slice. Red outlined recording electrode represents the electrode LFP used to trigger stimulation. B) schematic of stimulation triggered by rising LFP. C) the unfiltered LFP recorded from the red outlined electrode, averaged across stimulations, with gray shading indicating standard deviation. Black, dotted line represents the stimulation onset time. D) side-view of the change in spiking activity (0–10 ms post-stimulus) in log scale after stimulation.

most comprehensive tool to model network wide effects of optogenetic stimulation under diverse parameters.

Finally, we developed open and closed-loop stimulation protocols that permit users to model stimulation with versatile temporal and spatial properties. Each protocol can be used with electric field or optogenetic stimulation. Furthermore, though we only demonstrate STDP with paired-pulse stimulation, STDP can be enabled for each protocol. Simulations with STPD take much longer to run due to the extra overhead and calculations (e.g. paired-pulse stimulation with STDP takes 3 times longer to run than paired-pulse stimulation without STDP enabled), but they can provide information on how connection strengths could change under specific interventions. For instance, compared to pre-conditioning, after paired-pulse conditioning, we found that stimulation delivered at Site1 resulted in a 597 % larger LFP response at Site2 (Fig. 3). These results are similar to other population-based neuron simulation tools. For example, the integrate-and-fire model developed by Shupe and Fetz (2021) found a 600 % increase in evoked response after delivering paired pulse stimulation using a similar delay. More importantly, these results are congruent with *in-vivo* work showing that paired-pulse stimulation can strengthen connectivity between stimulation sites (Yazdan-Shahmorad et al., 2018; Seeman et al., 2017). Similar to paired-pulse conditioning, spatiotemporal patterned stimulation can be used to apply stimulation across many sites with differing delays and amplitudes between sites. This type of patterned stimulation might be particularly advantageous for treating neuropathologies, such as stroke and Alzheimer's, that result in aberrant network activity across multiple nodes. (Asp et al., 2023; Ip et al., 2021; Khateeb et al., 2019; Khateeb et al., 2022; Sato et al., 2022; Wang et al., 2013; Zhou et al., 2022; Zhou et al., 2023).

While paired-pulse and spatiotemporal stimulation are open-loop approaches, it is thought that a significant factor contributing to the inconsistent effects of neural stimulation is the variable brain states in which the stimulation is delivered (Bloch et al., 2019, 2022; Zrenner and Ziemann, 2024). Advancements in technology for rapidly processing ongoing neural activity have made it possible to deliver closed-loop stimulation during specific neural states. Providing support for cycle-triggered stimulation was motivated by several studies which found that delivering stimulation during a specific LFP phase resulted in larger stimulation evoked responses (Zanos et al., 2018; Zrenner and Ziemann, 2024; Zrenner et al., 2018, Wischnewski et al., 2022).

4.2. Comparison to other models

We chose to implement these features within the existing VERTEX software because unlike many other computational models that simulate spiking activity, LFPs, and synaptic plasticity in neurons, VERTEX uniquely does so in a large population of neurons using realistic biophysical properties. LFPy and The NEURON simulator are python-based models that predict spiking activity in highly realistic neuron models with more compartments and complex branching than VERTEX (Hines and Carnevale 1997; Lindén et al., 2010). However, both are designed to simulate activity in a single neuron or a very small collection of neurons. In contrast, The Brian simulator uses point neurons but can simulate activity in a large population of neurons and has support for synaptic plasticity including STDP (Goodman and Brette, 2009). Similarly, the integrate-and-fire model by Shupe and Fetz (2021) simulates point neurons without physical properties in several hundred neurons. It also incorporates STDP and various open- and closed-loop stimulation protocols. Despite advantageous features in other models, VERTEX's use of realistic neuron morphologies and connectivity, where dendritic and synaptic activity contribute to LFPs, generates more realistic LFPs. This is particularly important as it allows users to explore the relationship between spikes and LFPs, an area with limited *in-vivo* research (Ahmadi et al., 2021; Valero et al., 2017; Yazdan-Shahmorad et al., 2011; Yazdan-Shahmorad et al., 2013). By deepening our understanding of the correlations between spiking and LFPs, experimentalists could make greater use of LFP signals, which are obtained through less invasive methods.

4.3. Future directions

While our novel extensions provide comprehensive features to VERTEX, there is potential for further expansion and improvement of these simulations. In particular, our optogenetic stimulation model is based on several theoretical frameworks. More *in-vivo* research could refine these models to more accurately represent light spread through brain tissue, better account for light source parameters such as the optical fiber's numerical aperture, and improve photocurrent dynamics for more realistic onset mechanics and longer duration light pulses to accommodate both peak and plateau currents.

5. Conclusions

Our extensions to VERTEX provide a highly adaptable, comprehensive, and realistic platform for users to test and predict the effects of diverse neural stimulation methods on spiking activity and local field potentials. We anticipate that these extensions will be highly valuable in the fields of systems neuroscience and therapeutic neural interfaces.

These new features enable the exploration of numerous important questions, such as comparing the effects of optogenetic stimulation to electrical stimulation. At an individual level, for experimentalists, we hope these tools will serve as a preliminary means to predict local and network-level effects of modern stimulation methods before conducting *in-vivo* experiments. Doing so will reduce the number of extraneous hypotheses tested *in-vivo*, thereby saving costs, time, and reducing the use of animals.

CRediT authorship contribution statement

Larry Shupe: Writing – review & editing, Writing – original draft, Visualization, Validation, Methodology, Investigation, Formal analysis, Data curation, Conceptualization. **Julien Bloch:** Validation, Methodology, Conceptualization. **Eberhard Fetz:** Writing – review & editing, Validation, Supervision, Methodology, Investigation, Funding acquisition, Conceptualization. **Azadeh Yazdan-Shahmorad:** Writing – review & editing, Validation, Supervision, Resources, Methodology, Investigation, Funding acquisition, Conceptualization. **Anne F. Pierce:** Writing – review & editing, Writing – original draft, Visualization, Validation, Project administration, Methodology, Investigation, Formal analysis, Data curation, Conceptualization.

Declaration of Competing Interest

The authors declare the following financial interests/personal relationships which may be considered as potential competing interests: Azadeh Yazdan-Shahmorad reports financial support was provided by National Institutes of Health. Anne F. Pierce reports financial support was provided by National Institutes of Health. Larry Shupe reports financial support was provided by National Institutes of Health. Eberhard Fetz reports financial support was provided by National Institutes of Health. Azadeh Yazdan-Shahmorad reports financial support was provided by National Science Foundation. Azadeh Yazdan-Shahmorad reports financial support was provided by American Heart Association Inc. Anne F. Pierce reports financial support was provided by American Heart Association Inc. If there are other authors, they declare that they have no known competing financial interests or personal relationships that could have appeared to influence the work reported in this paper.

Acknowledgments

This work was funded by NIH R01NS119593, NSF 2223495, and the American Heart Association. We thank Riya Jain for her contribution to coding.

Code availability

All software needed to run model simulations and figure generation can be found at this code repository: https://github.com/lshupe/Vertex2_YL

Appendix A. Supporting information

Supplementary data associated with this article can be found in the online version at doi:10.1016/j.jneumeth.2025.110514.

Data availability

The code repository is listed within the manuscript

References

Ahmadi, N., Constandinou, T.G., Bouganis, C.S., 2021. Inferring entire spiking activity from local field potentials. Sci. Rep. 11, 19045. https://doi.org/10.1038/s41598-021-98021-9.

Asp, A.J., Chintaluru, Y., Hillan, S., Lujan, J.L., 2023. Targeted neuroplasticity in spatiotemporally patterned invasive neuromodulation therapies for improving clinical outcomes. Front. Neuroinform. 17, 1150157. https://doi.org/10.3389/fninf.2023.1150157.

Bi, G., Poo, M., 2001. Synaptic modification by correlated activity: Hebb's postulate revisited. Annu. Rev. Neurosci. 24, 139–166. https://doi.org/10.1146/annurev.neuro.24.1.139.

Bloch, J., 2023. Computational and experimental advances in clinically relevant neurostimulation of non-human primates. [Doctoral dissertation, University of Washington. ProQuest Dissertations Publishing.

Bloch, J., Greaves-Tunnell, A., Shea-Brown, E., Harchaoui, Z., Shojaie, A., Yazdan-Shahmorad, A., 2022. Network structure mediates functional reorganization induced by optogenetic stimulation of non-human primate sensorimotor cortex. iScience 25, 104285. https://doi.org/10.1016/J.ISCI.2022.104285.

Bloch, J.A., Khateeb, K., Silversmith, D.B., O'Doherty, J.E., P. N. Sabes, P.N., Yazdan-Shahmorad, A., 2019. Cortical stimulation induces Network-Wide coherence change in Non-Human primate somatosensory cortex. EMBC 6446–6449. https://doi.org/10.1109/EMBC.2019.8856633.

Brette, R., Gerstner, W., 2005. Adaptive exponential Integrate-and-Fire model as an effective description of neuronal activity. J. Neurophysiol. 94 (5), 3637–3642. https://doi.org/10.1152/jn.00686.2005.

Chuong, A.S., Miri, M.L., Busskamp, V., Matthews, G.A.C., Acker, L.C., Sørensen, A.T., Young, A., Klapoetke, N.C., Henninger, M.A., Kodandaramaiah, S.B., Ogawa, M., Ramanlal, S.B., Bandler, R.C., Allen, B.D., Forest, C.R., Chow, B.Y., Han, X., Lin, Y., Tye, K.M., Roska, B., Cardin, J.A., Boyden, E.S., 2014. Noninvasive optical inhibition with a red-shifted microbial rhodopsin. Nat. Neurosci. 17, 1123–1129. https://doi.org/10.1038/nn.3752.

Deisseroth, K., 2015. Optogenetics: 10 years of microbial opsins in neuroscience. Nat. Neurosci. 18, 1213–1225. https://doi.org/10.1038/nn.4091.

Foutz, T.J., Arlow, R.L., McIntyre, C.C., 2012. Theoretical principles underlying optical stimulation of a channelrhodopsin-2 positive pyramidal neuron. J. Neurophysiol. 107 (12), 3235–3245. https://doi.org/10.1152/jn.00501.2011.

Gao, T.T., Oh, T.J., Mehta, K., Huang, Y.A., Camp, T., Fan, H., Han, J.W., Barnes, C.M., Zhang, K., 2023. The clinical potential of optogenetic interrogation of pathogenesis. Clin. Transl. Med. 13 (5), e1243. https://doi.org/10.1002/ctm2.1243.

Goodman, D.F., Brette, R., 2009. The brian simulator. Front. Neurosci. 3 (2), 192–197. https://doi.org/10.3389/neuro.01.026.2009.

Gupta, N., Bansal, H., Roy, S., 2019. Theoretical optimization of high-frequency optogenetic spiking of red-shifted very fast-Chrimson-expressing neurons. Neurophotonics 6 (2), 025002. https://doi.org/10.1117/1.NPh.6.2.025002.

Ip, Z., Rabiller, G., He, J.W., Chavan, S., Nishijima, Y., Akamatsu, Y., Liu, J., Yazdan-Shahmorad, A., 2021. Local field potentials identify features of cortico-hippocampal communication impacted by stroke and environmental enrichment therapy. Journal of Neural Engineering 18 (4). https://doi.org/10.1088/1741-2552/ac0a54.

Khateeb, K., Bloch, J., Zhou, J., Rahimi, M., Griggs, D.J., Kharazia, V.N., Le, M.N., Wang, R.K., Yazdan-Shahmorad, A., 2022. A versatile toolbox for studying cortical physiology in primates. Cell Rep. Methods 2 (3), 100183. https://doi.org/10.1016/j.crmeth.2022.100183.

Khateeb, K., Yao, Z., Kharazia, V.N., Burunova, E.P., Song, S., Wang, R., Yazdan-Shahmorad, A., 2019. A practical method for creating targeted focal ischemic stroke in the cortex of nonhuman primates. EMBC 3515–3518. https://doi.org/10.1109/EMBC.2019.8857741.

Klapoetke, N., Murata, Y., Kim, S., Pulver, S.R., Birdsey-Benson, A., Cho, Y.K., Morimoto, T.K., Chuong, A.S., Carpenter, E.J., Tian, Z., Wang, J., Xie, Y., Yan, Z., Zhang, Y., Chow, B.Y., Surek, B., Melkonian, M., Jayaraman, V., Constantine-Paton, M., Wong, G.K., Boyden, E.S., 2014. Independent optical excitation of distinct neural populations. Nat. Methods 11, 338–346. https://doi.org/10.1038/nmeth.2836.

Mattis, J., Tye, K., Ferenczi, E., Ramakrishnam, C., O'Shea, D.J., Prakash, R., Gunaydin, L.A., Hyun, M., Fenno, L.E., Gradinaru, V., Yizhar, O., Deisseroth, K., 2012. Principles for applying optogenetic tools derived from direct comparative analysis of microbial opsins. Nat. Methods 9, 159–172. https://doi.org/10.1038/nmeth.1808.

Saran, S., Gupta, N., Roy, S., 2018. Theoretical analysis of low-power fast optogenetic control of firing of Chronos-expressing neurons. Neurophotonics 5 (2), 025009. https://doi.org/10.1117/1.NPh.5.2.025009.

Sato, Y., Schmitt, O., Ip, Z., Rabiller, G., Omodaka, S., Tominaga, T., Yazdan-Shahmorad, A., Liu, J., 2022. Pathological changes of brain oscillations following ischemic stroke. Journal of Cerebral Blood Flow & Metabolism 42 (10), 1753–1776. https://doi.org/10.1177/0271678X221105677.

Seeman, S.C., Mogen, B.J., Fetz, E.E., Perlmutter, S.I., 2017. Paired stimulation for Spike-Timing-Dependent plasticity in primate sensorimotor cortex. J. Neurosci. 37 (7), 1935–1949. https://doi.org/10.1523/JNEUROSCI.2046-16.2017.

Senova, S., Scisniak, I., Chiang, C.C., Doignon, I., Palfi, S., Chaillet, A., Martin, C., Pain, F., 2017. Experimental assessment of the safety and potential efficacy of high irradiance photostimulation of brain tissues. Sci. Rep. 7, 43997. https://doi.org/10.1038/srep43997.

Shupe, L., Fetz, E.E., 2021. An integrate-and-fire spiking neural network model simulating artificially induced cortical plasticity. ENeuro, 0333-20.

Sivagnanam, S., Majumdar, A., Yoshimoto, K., Astakhov, V., Bandrowski, A., Martone, M. E., Carnevale, N.T., 2013. Introducing the neuroscience gateway. IWSG 993.

Thornton, C., Hutchings, F., Kaiser, M., 2019. The virtual electrode recording tool for EXtracellular potentials (VERTEX) version 2.0: modelling in vitro electrical stimulation of brain tissue. [version 1; peer review: 2 approved]. Wellcome Open Res. 4, 20. https://doi.org/10.12688/wellcomeopenres.15058.1.

Tomsett, R.J., Ainsworth, M., Thiele, A., Sanayei, M., Chen, X., Gieselmann, M.A., Whittington, M.A., Cunningham, M.O., Kaiser, M., 2015. Virtual electrode recording tool for EXtracellular potentials (VERTEX): comparing multi-electrode recordings from simulated and biological mammalian cortical tissue. Brain Struct. Funct. 220, 2333–2353. https://doi.org/10.1007/s00429-014-0793-x.

Valero, M., Averkin, R.G., Fernandez-Lamo, I., Aguilar, J., Lopez-Pigozzi, D., Brotons-Mas, J.R., Cid, E., Tamas, G., de la Prida, L.M., 2017. Mechanisms for selective single-cell reactivation during offline sharp-wave ripples and their distortion by fast ripples. Neuron 94 (6), 1234–1247. https://doi.org/10.1016/j.neuron.2017.05.032.

Wang, J., Zuo, X., Dai, Z., Xia, M., Zhao, Z., Zhao, X., Jia, J., Han, Y., He, Y., 2013. Disrupted functional brain connectome in individuals at risk for Alzheimer's disease. Biological Psychiatry 73 (5), 472–481. https://doi.org/10.1016/j.biopsych.2012.03.026.

Wischnewski, M., Haigh, Z.J., Shirinpour, S., Alekseichuk, I., Opitz, A., 2022. The phase of sensorimotor mu and beta oscillations has the opposite effect on corticospinal excitability. Brain Stimul. 15 (5), 1093–1100. https://doi.org/10.1016/j.brs.2022.08.005.

Yazdan-Shahmorad, A., Kipke, D.R., Lehmkuhle, M.J., 2011. Polarity of cortical electrical stimulation differentially affects neuronal activity of deep and superficial layers of rat motor cortex. Brain Stimul. 4 (4), 228–241. https://doi.org/10.1016/j.brs.2010.11.004.

Yazdan-Shahmorad, A., Kipke, D.R., Lehmkuhle, M.J., 2013. High γ power in ECoG reflects cortical electrical stimulation effects on unit activity in layers V/VI. J. Neural Eng. 10 (6), 066002. https://doi.org/10.1088/1741-2560/10/6/066002.

Yazdan-Shahmorad, A., Silversmith, D.B., Kharazia, V., Sabes, P.N., 2018. Targeted cortical reorganization using optogenetics in non-human primates. eLife 7, e31034. https://doi.org/10.7554/eLife.31034.

Yizhar, O., Fenno, L.E., Davidson, T.J., Mogri, M., Deisseroth, K., 2011. Optogenetics in neural systems. Neuron 71 (1), 9–34. https://doi.org/10.1016/j.neuron.2011.06.004.

Yuan, Y., Zheng, L., Feng, Z., Yang, G., 2021. Different effects of monophasic pulses and biphasic pulses applied by a bipolar stimulation electrode in the rat hippocampal CA1 region. BioMed. Eng. OnLine 20, 25. https://doi.org/10.1186/s12938-021-00862-y.

Zanos, S., Rembado, I., Chen, D., Fetz, E.E., 2018. Phase-locked stimulation during cortical beta oscillations produces bidirectional synaptic plasticity in awake monkeys. Curr. Biol. 28, 2515–2526.

Zhou, J., Khateeb, K., & Yazdan-Shahmorad, A. (2023). Early Intervention with Electrical Stimulation Reduces Neural Damage After Stroke in Non-human Primates. *bioRxiv: the preprint server for biology*,12.18.572235. https://doi.org/10.1101/2023.12.18.572235.

Zhou, J., Khateeb, K., Gala, A., Rahimi, M., Griggs, D.J., Ip, Z., Yazdan-Shahmorad, A., 2022. Neuroprotective effects of electrical stimulation following ischemic stroke in non-human primates. IEEE, pp. 3085–3088. https://doi.org/10.1109/EMBC48229.2022.9871335.

Zrenner, C., Desideri, D., Belardinelli, P., Ziemann, U., 2018. Real-time EEG-defined excitability states determine efficacy of TMS-induces plasticity in human motor cortex. Brain Stimul. 11 (2), 374–389. https://doi.org/10.1016/j.brs.2017.11.016.

Zrenner, C., Ziemann, U., 2024. Closed-loop brain stimulation. Biol. Psychiatry 95 (6), 545–552. https://doi.org/10.1016/j.biopsych.2023.09.014.